Simplex based three-dimensional eigenray search for underwater predictions

Rogério de Moraes Calazan[a] and Orlando Camargo Rodríguez

LARSyS, Campus de Gambelas, University of Algarve, Faro, PT-8005-139, Portugal

A solution for the calculation of three-dimensional (3D) eigenrays based on Simplex optimization, implemented in a 3D Gaussian beam model, is investigated in this paper. The validation and performance of the solution were analyzed through comparisons against an equivalent (flat) two-dimensional waveguide, and against results of a tank scale experiment presented in Sturm and Korakas [(2013). J. Acoust. Soc. Am. **133**(1), 108–118], in which cross-slope propagation in a wedge waveguide with a mild slope was considered. It was found that the search strategy based on Simplex optimization was able to calculate efficiently and accurately 3D eigenrays, thus providing predictions of arrival patterns along cross-slope range, which replicated elaborate patterns of mode shadow zones, intra-mode interference, and mode arrivals. A remarkable aspect of the search strategy was its ability to provide accurate values of initial eigenray elevation and azimuth, within the accuracy defined for the eigenray to arrive at the location of a given hydrophone.
© 2018 Acoustical Society of America. https://doi.org/10.1121/1.5030922

I. INTRODUCTION

Eigenrays can be defined as particular rays that for a given waveguide geometry connect the source to the receiver (Jensen *et al.*, 2011). The accurate calculation of eigenrays is a problem of great interest in underwater acoustics because they can be used for faithful predictions of the received signal, which is extremely sensitive to the ray travel time and ray take-off angles. In two-dimensional (2D) waveguides, the problem can be solved efficiently using root finder algorithms in one dimension; in such cases, the problem can be stated as searching for the zeros of a function, which depends only on the elevation angles. The extension of such root finder algorithms to find eigenrays in a three-dimensional (3D) waveguide is a cumbersome task that requires the search to take place on the 2D plane of elevation and azimuth, and would be guided mainly by the minimization of the distance between the final position of the ray and the position of the hydrophone; besides, looking for the minima on the elevation/azimuth plane, unlike the one-dimensional search, cannot take place along a particular direction due to the complex regime of propagation, which often needs to account for out-of-plane effects, non-linear internal waves or boundary features (Buckingham, 1987; Tolstoy, 1996). The problem is also computationally demanding, since it often relies on the shooting of a large amount of initial rays (Calazan *et al.*, 2017). Some of the approaches described in the literature relied on interpolation (Xing *et al.*, 2013), or ray computations using spherical coordinates (Reilly *et al.*, 2016); the latter was noticed to be of low accuracy and less efficient than the equivalent search using Cartesian coordinates; a drawback of the previous discussions is that both considered basic idealized waveguides and a single hydrophone. An analytic approach to the problem was proposed in Maltsev (2001), which stated the calculation of eigenrays as a variational problem. Thus, finding an initial set of eigenrays for a receiver close to the source allowed eigenrays to be found for an arbitrary receiver position; caustics could be taken into account by considering a ray amplitude, which was frequency dependent. However, the numerical implementation of the method for general sound profiles required the introduction of parameterized smoothing functions, and the performance of the method accounting for 3D bathymetries was not considered. A summation approach, based on the superposition of complex source beams, discussed in detail in Heilpern *et al.* (2007) and Gluk and Heyman (2011), proposes to rely on beam shooting to avoid eigenray calculations; to this end, the beams need to be properly collimated through the proper selection of beam parameters for the given geometry of propagation. The discussion, however, was limited to 2D propagation and did not account for boundary reflections. In contrast, the approach considered in this paper relies on a small set of parameters (which needs to be determined only once) and is able to handle arbitrary 3D effects, induced by either sound speed distributions or bathymetries (or both). The computational strategy of Simplex optimization was designed in order to rely on an efficient selection, within the original region of candidates that encloses a given receiver, such that the search can be accomplished efficiently with either a vertical or a horizontal array. In fact, Simplex optimization guides the ray solution accounting for all environmental influences, finding take-off angles that allow a given ray to pass nearby the receiver within a user-defined distance. In this context, the method provides an accurate estimate of travel time, which is fundamental to predict the channel impulse response.

The Simplex optimization was implemented in the TRACEO3D Gaussian beam model (Rodriguez *et al.*, 2017); preliminary results were compared against predictions from

a)Electronic mail: a53956@ualg.pt

the 2D TRACEO model (Rodriguez *et al.*, 2012) for an equivalent (flat) waveguide. Results from a tank scale experiment reported in Sturm and Korakas (2013) were considered for validation and performance assessment. The organization of this paper is as follows: Simplex-based eigenray search is presented in Sec. II, the TRACEO3D model is compactly described in Sec. III, while Sec. IV presents the experimental model validation. Conclusions and future work are presented in Sec. V.

II. THE EIGENRAY SIMPLEX-BASED SEARCH

The 3D search of eigenrays is composed of three different strategies: first, to start the search determine a reliable candidate region that encloses the receiver; second, apply the general rules of Simplex optimization using the candidate region to find an eigenray; third, avoid the storage of duplicated eigenrays. These strategies are discussed in the following sections.

A. Selection of a reliable candidate region

Let θ and ϕ be the ray elevation and azimuth, respectively. For a given set of receivers, the initial choice of take-off angles (defined by a set of θ and ϕ at the source) depends on many waveguide features, such as boundary variations over the horizontal plane, source-receiver alignment, and the existence or absence of environmental variations. In any case, a given choice should aim at sweeping the waveguide in such a way that a large number of rays should propagate among all receivers, and thus enough eigenrays can be found at every receiver to predict accurately the corresponding impulse response. For a given receiver, a vertical plane is calculated using the normal vector connecting the source to the receiver, and the crossings of rays through the plane determine the closest distance from each ray to the receiver. Let θ_i and ϕ_j define the take-off angle of the (i, j)th ray; a candidate search space is then build with the region defined by the corners

$$\begin{bmatrix} \theta_i, \phi_j & \theta_i, \phi_{j+1} \\ \theta_{i+1}, \phi_j & \theta_{i+1}, \phi_{j+1} \end{bmatrix}.$$

These corners are changed over iterations according to the following rules:

- Fix i and increment j until the horizontal deviation of the closest distance vanishes;
- Increment i and repeat the previous step until it covers the vertical deviations.

At each iteration, a new search region is created; the corresponding corners are used to divide the region in triangles using four combinations

(1) $[\theta_i, \phi_j \quad \theta_{i+1}, \phi_j \quad \theta_i, \phi_{j+1}]$;
(2) $[\theta_i, \phi_j \quad \theta_{i+1}, \phi_j \quad \theta_{i+1}, \phi_{j+1}]$;
(3) $[\theta_i, \phi_j \quad \theta_i, \phi_{j+1} \quad \theta_{i+1}, \phi_{j+1}]$;
(4) $[\theta_{i+1}, \phi_j \quad \theta_i, \phi_{j+1} \quad \theta_{i+1}, \phi_{j+1}]$.

To determine which triangle contains the receiver, the method calculates the barycentric coordinates λ, which are given by

$$\begin{pmatrix} x_1 & x_2 & x_3 \\ y_1 & y_2 & y_3 \\ z_1 & z_2 & z_3 \end{pmatrix} \lambda = \begin{pmatrix} x_r \\ y_r \\ z_r \end{pmatrix}, \tag{1}$$

where (x_1, y_1, z_1), (x_2, y_2, z_2), and (x_3, y_3, z_3) represent the coordinates of the triangle vertex, and (x_r, y_r, z_r) are the coordinates of the receiver. The search considers all triangles divisions; it decides that the receiver lies inside a given triangle when the components of the normalized λ are all positive. When this happens, the take-off angles (θ, ϕ) of the corresponding vertex are considered for further Simplex optimization. Figure 1 depicts the candidate region where a hypothetical receiver is located at the first combination of launching angles. Although the triangles overlap, the search must consider all of them, until the one containing the receiver is found. This selection step is fundamental in order to overcome the chaotic distribution of vertex corners induced by the waveguide. In the general case, rays from an initial narrow pyramid will end up producing an amorphous cloud of corners near the receiver, with consecutive rays following completely different paths. For instance, one corner can be produced by a ray coming from the bottom, while another corner can be produced by a ray coming from the surface.

B. Simplex optimization

The Simplex method was developed as a general strategy to optimize a function of N variables (Nelder and Mead, 1965). A simplex can be idealized as a geometric figure in N dimensions, defined by a set of $N+1$ points; for instance, a simplex is a triangle in two dimensions, and in three dimensions a simplex is a tetrahedron. The method can be able to
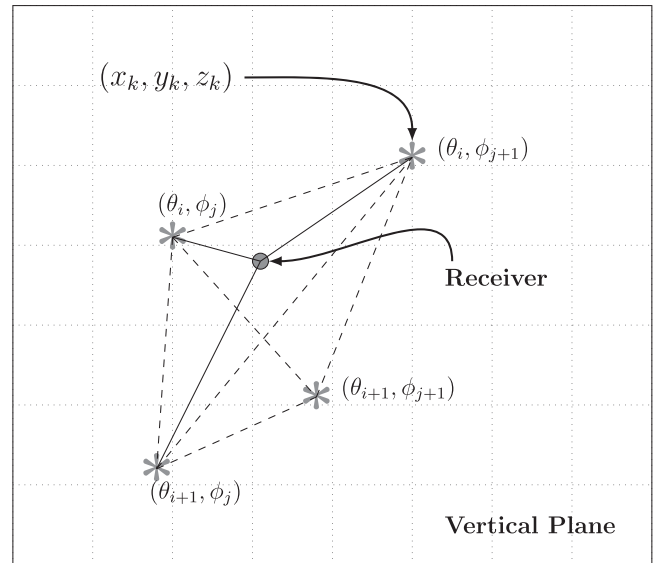

FIG. 1. Candidate region with four corners, represented as asterisks, and coordinates (x_k, y_k, z_k) where a given ray intersects the vertical plane associated to the receiver. The region is divided into triangles (dashed lines), and barycentric coordinates (solid lines) λ_1, λ_2, and λ_3 are used to determine which triangle contains the receiver.

Rogério de Moraes Calazan and Orlando Camargo Rodríguez

achieve convergence in few iterations, and requires few function evaluations, a feature which is important when dealing with complicated objective functions (Lagarias *et al.*, 1998).

Within the context of eigenray search the objective function to be minimized can be defined as

$$f(\theta, \phi) = \sqrt{\begin{array}{c}[x_r - x(\theta, \phi)]^2 + \\ [y_r - y(\theta, \phi)]^2 + \\ [z_r - z(\theta, \phi)]^2\end{array}}, \qquad (2)$$

where $x(\theta, \phi)$, $y(\theta, \phi)$, and $z(\theta, \phi)$ represent the ray coordinates on the vertical plane of the receiver. The selection of a candidate region delivers a high quality initial guess suited for the simplex algorithm, which will compute a point between each vertex of the triangle and its centroid. The new point will produce a simplex with the same triangular shape inside the initial region. Additionally, overlapping triangles can be used to restart the optimization in regions in which the convergence is failing. Once the simplex is started, it uses three operations called reflection, contraction, and expansion, based on the simplex centroid, to determine a new vertex with smaller values of $f(\theta, \phi)$. The optimization stops when the value of the function at a latest vertex is below a predefined threshold, and the corresponding pair (θ, ϕ) is used to calculate the eigenray. Associated with those operations, there is a set of reflection, expansion, and contraction coefficients: α, γ, and β, respectively. During initial tests for a single receiver, the algorithm achieved a remarkable convergence with $\alpha = 1.5$, $\gamma = 1.65$, and $\beta = 0.5$. Those values were found to guarantee the convergence of the method for all eigenray calculations of the different experimental configurations considered. It should be noticed that parallel tests using swarm optimization, with different combinations of its own specific parameters, failed often to achieve the desired accuracy, besides requiring significant amounts of computational time.

C. Avoiding storage of duplicated eigenrays

A blind application of Simplex optimization can lead to the calculation of the same eigenray using different candidate regions. To avoid this, the following additional tests were introduced:

- Once an eigenray is found, it is verified that the corresponding pair (θ, ϕ) lies inside the candidate region. If the condition is not fulfilled the eigenray is discarded.
- As eigenrays are being calculated, the corresponding information regarding (θ, ϕ) together with surface and bottom reflections are stored in memory; each new eigenray is compared against those in memory and discarded if already present.

A final procedure for sorting the computed eigenrays by time is required to represent the channel impulse response.

III. THE TRACEO3D GAUSSIAN BEAM MODEL

The Simplex based eigenray search was implemented in the TRACEO3D Gaussian beam model (Rodriguez *et al.*, 2017),

which is a 3D extension of the TRACEO model (Rodriguez *et al.*, 2012). TRACEO3D relies on the 3D solution of the Eikonal equations to calculate ray trajectories, and on the solution of the dynamic equations to calculate ray amplitudes (Červený and Pšenčík, 1979; Collins and Kuperman, 1991; Jensen *et al.*, 2011; Popov, 2002). For a given eigenray, such amplitude can be written as

$$A(s) = \frac{1}{4\pi} \sqrt{\frac{c(s)}{c(0)} \frac{\cos \theta(0)}{\det \boldsymbol{Q}(s)}} \exp[-i\omega\tau(s)], \qquad (3)$$

where s corresponds to the ray arc length, and $c(s)$ and $\tau(s)$ stand for the sound speed and travel time along the ray, respectively; the complex matrix $\boldsymbol{Q}(s)$ describes the beam spreading.

IV. VALIDATION

The accuracy and efficiency of the Simplex based eigenray search in three-dimensions was intensively tested with comparisons against an equivalent 2D waveguide, and against results from a tank scale experiment. The experiment and comparisons are discussed in the following sections.

A. The tank scale experiment

Environmental measurements and geometric parameters from the tank scale experiment discussed in Korakas *et al.* (2009) and Sturm and Korakas (2013) were considered for the validation of model predictions. The inner tank dimensions were 10 m long, 3 m wide, and 1 m deep. The source and the receiver were both aligned along the across-slope direction, as shown in Fig. 2. The transmitted signal was a five-cycle pulse with a Gaussian envelope, with a frequency spectrum showing a main lobe centered at 150 kHz and 100 kHz bandwidth. The bottom was filled with sand and a rake was used to produce a mild slope angle $\alpha \approx 4.5°$. Bottom parameters corresponded to $c_p = 1700$ m/s, $\rho = 1.99$ g/cm^3, and $\alpha_p = 0.5$ dB/λ. The receiver was located at 10 mm depth from the surface, bottom
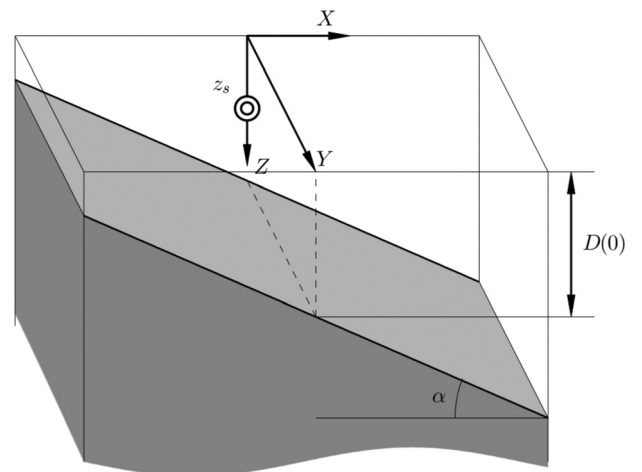

FIG. 2. Cross-slope geometry: α correspond to the bottom slope, $D(0)$ is the bottom depth at the source position, z_s stands for the acoustical source depth where the double circle indicates its position, and the synthetic horizontal array is located along the Y-axis.

J. Acoust. Soc. Am. **143** (4), April 2018

Rogério de Moraes Calazan and Orlando Camargo Rodríguez   2061

depth at source position stands for $D(0) = 48$ mm. The ASP-H data set of cross-slope propagation is composed of time signals, recorded at a fixed receiver depth denominated z_r, and source/receiver distances starting from $Y = 0.1$ m until $Y = 5$ m in increments of 0.005 m, providing a sufficiently fine representation of the acoustic field in terms of range. Three different source depths were considered, namely $z_s = 10$ mm, 19 mm, and 26.9 mm, corresponding to data subsets referenced as ASP-H1, ASP-H2, and ASP-H3, respectively. Sound speed in the water was considered constant and corresponded to 1488.2 m/s for ASP-H1 and 1488.7 m/s for ASP-H2 and ASP-H3. For simulations purposes, a scale factor of 1000:1 is required to properly account in the model for the frequencies and lengths of the experimental configuration. Thus, experimental frequencies in kHz become model frequencies in Hz, and experimental lengths in mm become model lengths in m. For instance, an experimental frequency of 150 kHz becomes a model frequency of 150 Hz, and an experimental distance of 10 mm becomes a model distance of 10 m. Sound speed remains unchanged, as well as compressional and shear attenuations.

B. Numerical predictions and comparisons

A preliminary set of comparisons was performed between TRACEO3D and TRACEO considering the experimental setup described in the previous section. Models predictions were obtained for a source frequency of 150 Hz. The horizontal array was idealized starting at 0.1 km until 5 km in increments of 0.1 km. A *synthetic* five-cycle pulse with a Gaussian envelope was considered as the emitted signal. The received signal was computed using the model output of amplitudes and delays for each receiver range and depth. Only frequencies between 100 Hz and 200 Hz were considered; outside this interval, the acoustic field was set to zero. The signal in the time domain was calculated using the inverse Fourier transform.

Preliminary TRACEO3D predictions failed to produce satisfactory results using the parameters provided by the refinement discussed in Sturm and Korakas (2013); therefore, alternative geometries were considered. The configuration shown in Table I was found to replicate best the results presented in Fig. 3 from the above reference. 3D predictions, together with equivalent TRACEO calculations for a flat waveguide, are shown in Fig. 3. Simple visual inspection shows that the given set of parameters allows TRACEO3D [see Figs. 3(d)–3(f)] to predict the features visible in the experimental data, such as the numbers and position of the modes, as well as mode shadow zones, intra-mode interference, and mode arrivals. The only exception was the attempted replication of the ASP-H3 data set; it is believed

TABLE I. Geometric parameters used in numerical predictions of the waveguide used in ASP-H data sets.

	z_s (m)	z_r (m)	$D(0)$ (m)	Slope (%)
ASP-H1	6.7	11.0	43.9	4.5
ASP-H2	15.0	11.0	43.9	4.5
ASP-H3	27.0	11.0	43.9	4.5

that most of the discrepancies are due to the proximity of the source to the bottom in the corresponding geometry.

As suggested in Weinberg and Burridge (1974), Harrison (1979), and Buckingham (1987), such 3D effects can be explained based on ray/mode analogies. A mode can be considered as a standing wave in the vertical plane, and as a traveling wave describing a hyperbolic path on the horizontal plane, with the ray propagating itself initially upslope; at some point in range, the hyperbolic path crosses the across-slope direction. This analogy is fundamental for the discussion that follows. Predictions of normalized amplitudes for 2D and 3D calculations, regarding the ASP-H1 configuration, are shown in Fig. 4. The 3D results in the figure also indicate the modes in the (θ, ϕ) plane, allowing to determine take-off angles for different modes. The dashed lines represent approximately the edges of the shadow zones for each mode, with each shadow zone being a complex function of different parameters, such as frequency, wedge slope, and bottom properties. The across-slope direction where the source is aligned with the synthetic horizontal array is taken as $\phi = 0$; this angle increases towards the wedge apex.

The waveforms presented in Fig. 3(a) correspond to 2D predictions for the ASP-H1 configuration, with a source depth of 6.7 m. At short ranges, the predicted time signals seem to merge altogether. Above a certain range, they start to be separated, increasing the relative time delay between them as the receiver moves away from the source. As a receiver approaches the range of 5 km, late arrivals progressively lose more energy. Similar patterns can be seen in the other two configurations [see Figs. 3(b) and 3(c)]. The ASP-H1 2D prediction is further supported by Figs. 4(a)–4(e), in which the behavior of amplitudes over range exhibits a typical distribution for a flat waveguide: amplitudes can be seen to decrease steadily over elevations θ, while the number of eigenrays increases with range. Such steady decay can be explained by taking into account that 2D eigenrays are confined exclusively to the vertical plane, and thus bounce often off the bottom, losing more and more energy as elevation and range increase. A completely different pattern can be seen in Fig. 3(d), in which the waveforms were calculated accounting for full 3D effects. The figure shows an interesting pattern of mode arrivals: above 2 km, the modes $M1$ and $M2$ exhibit well resolved first and second arrivals, and the time delay between them decreases as the receiver moves away from the source; near 2 km, the expected first and second arrivals from mode $M3$ merge together, and the mode quickly vanishes due to the transition of $M3$ into a shadow zone; additionally, as range decreases below 2 km, modal refraction on the horizontal plane is such that the mode $M4$ becomes well resolved in time, but exhibiting only a single arrival. Similar modal patterns can be seen in Figs. 3(e) and 3(f). All mentioned features can be explained in more detail in Figs. 4(f)–4(j), which show that higher order modes are more intensively refracted at short ranges due to their large initial elevation θ; such modes rapidly bounce the bottom at the critical angle and thus vanish (i.e., enter a shadow zone) after being absorbed. Low order modes, on the other hand, are able to produce first and second arrivals at larger ranges

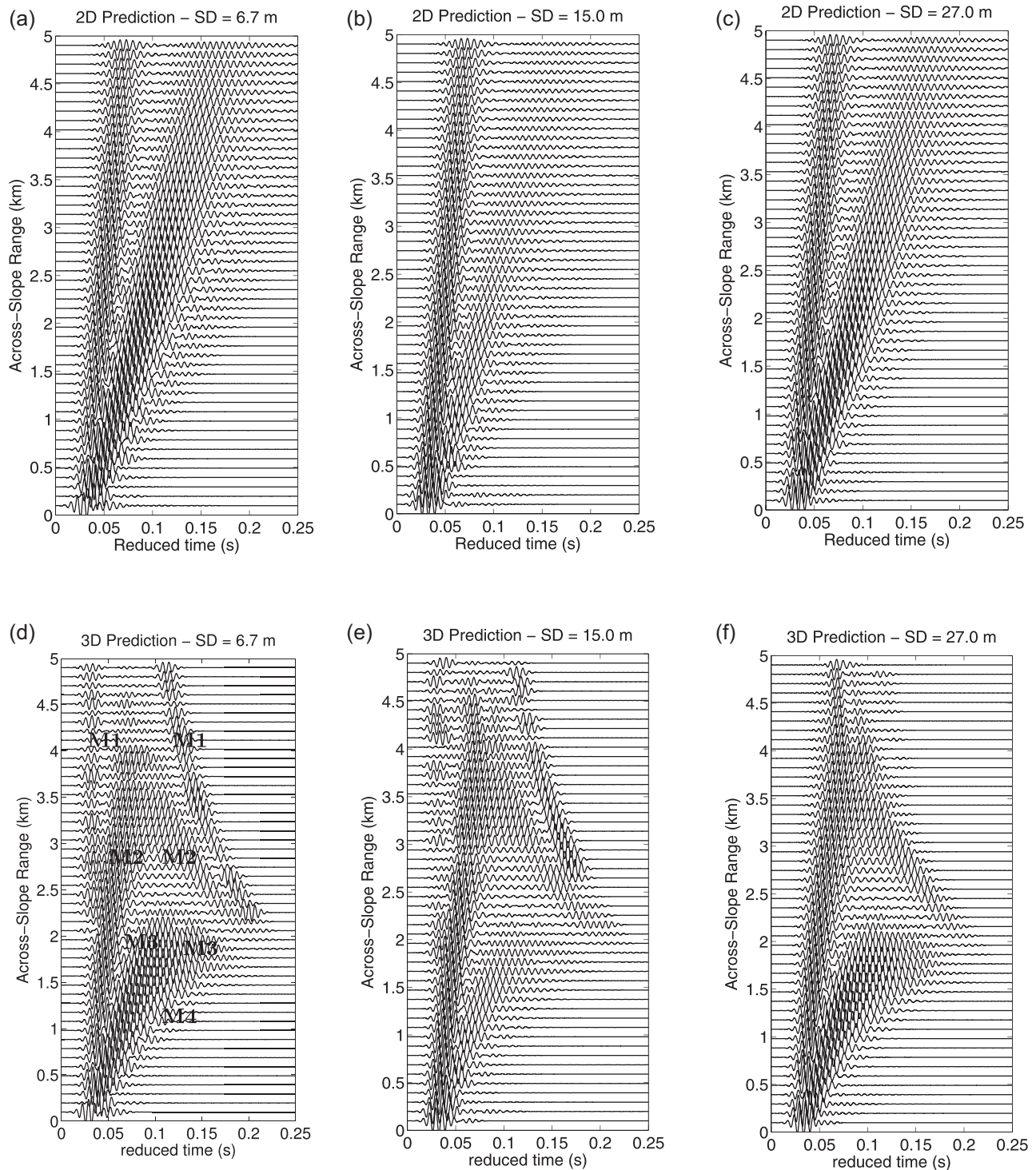Rogério de Moraes Calazan and Orlando Camargo Rodríguez

FIG. 3. Arrival pattern predictions calculated with TRACEO (top) and TRACEO3D (bottom) for the geometry presented in Table I; four modes can be identified regarding 3D predictions for the ASP-H1 configuration.

due to an interesting combination of propagation conditions: for a single "small" elevation θ, one can find a pair of azimuths ϕ_1 and ϕ_2 (with $\phi_1 < \phi_2$), in which the ray with take-off angles (θ, ϕ_2) propagates over shallower regions, but bounces more often off the bottom than the ray propagating with angles (θ, ϕ_1), and therefore leaks energy more rapidly. Thus, the entire 3D set of eigenray, travel time, and amplitude calculations allows the establishment of a remarkable connection between eigenray azimuth/elevation (θ, ϕ), mode order n, and receiver range r, with the parameters (θ, ϕ, n) increasing simultaneously as r decreases. These general conclusions, based mostly on ray theory, coincide with the discussion presented in Korakas *et al.* (2009). Obviously, there are some amplitude discrepancies between the results shown in Figs. 3(d) and 3(f) and those presented in Fig. 3 from Sturm and Korakas (2013); the discrepancies were in fact expected. During the calculations of arrival patterns, different synthetic pulses were considered besides the Gaussian
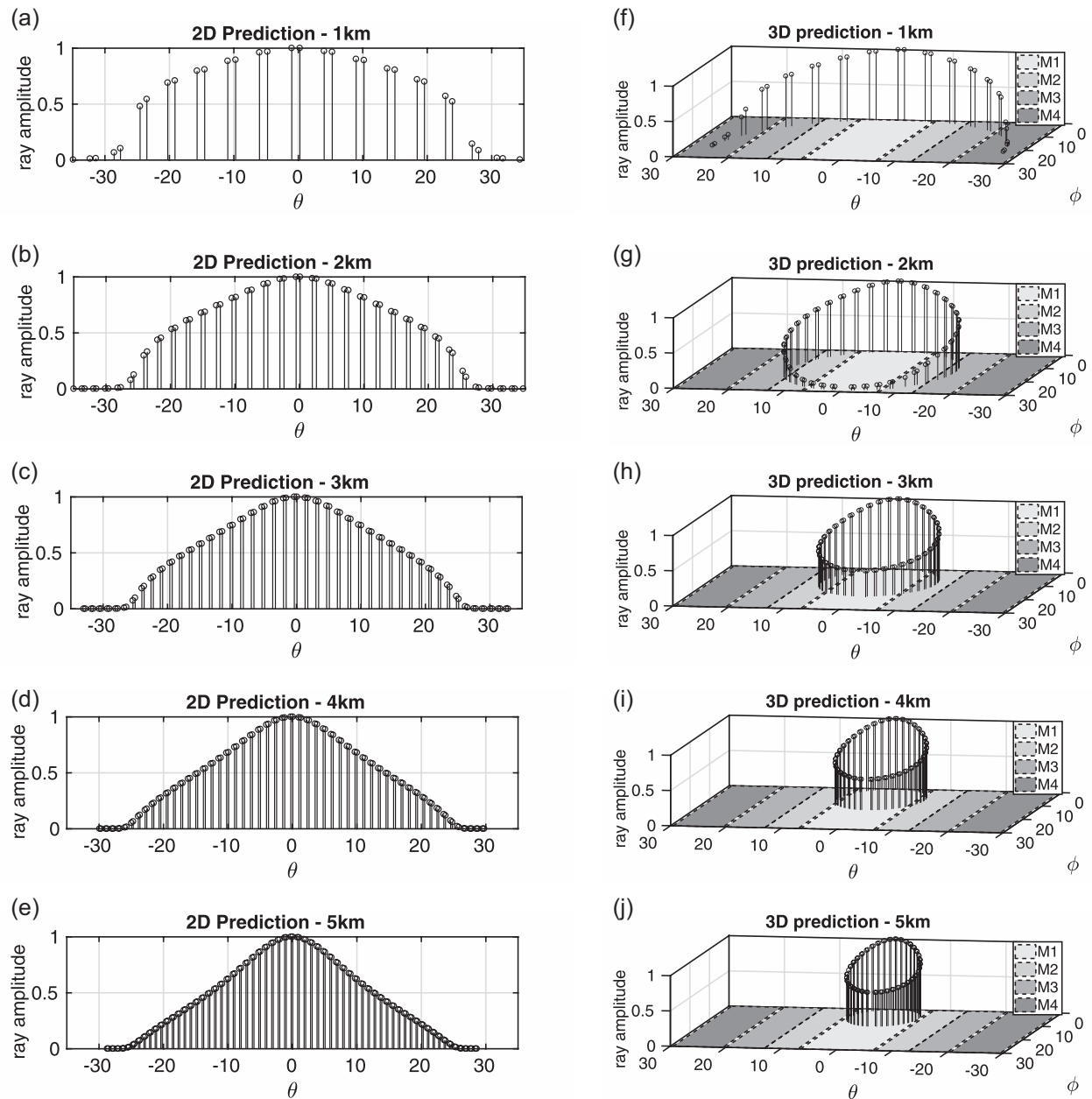
FIG. 4. Predictions of normalized amplitudes versus launching angles for the ASP-H1 configuration over range: TRACEO (left); TRACEO3D (right). The corresponding regions where modes can exist are indicated over the (θ, ϕ) plane. The dashed lines stand roughly for the critical launching angle.

one; it was found that the structure of propagating modes was highly sensitive to the particular choice of emitted signal. Such sensitivity can perhaps explain the usage of the recorded transmitted signal, instead of the synthetic one, to predict the arrival patterns shown in Sturm and Korakas (2013). A final insight into the problem can be found in the comparison of eigenrays, calculated with TRACEO for the flat case, and calculated with TRACEO3D for the wedge waveguide (see Fig. 5). At a first glance, there seems to be a perfect one-to-one correspondence of eigenrays in terms of elevations θ, and thus one could expect both 2D and 3D amplitudes to exhibit a similar correspondence. In fact, that is not the case; in the wedge waveguide, most eigenrays propagating up then down slope are bouncing on regions where bottom depth is smaller than the one of the 2D waveguide; as a consequence, instead of spreading progressively

over elevations as shown in Fig. 4(b), the amplitudes of arrivals become clustered between the limits of an elevation interval, as shown in Fig. 4(g).

V. CONCLUSIONS AND FUTURE WORK

The discussion presented in this paper demonstrated the feasibility of using the Simplex method to find 3D eigenrays. The method was implemented in the TRACEO3D Gaussian beam model, and the corresponding validation was carried out against predictions from the 2D TRACEO model, and against results from a tank scale experiment. The 3D predictions exhibited a remarkable similarity with most experimental features, replicating mode shadow zones, intra-mode interference, and mode arrivals; important connections in the ray/mode equivalence framework were noticed. TRACEO
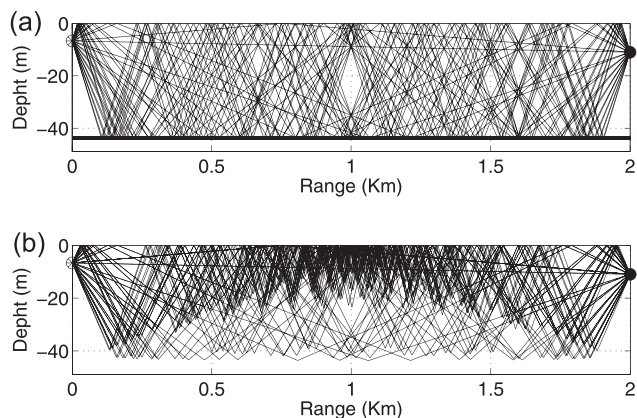
Rogério de Moraes Calazan and Orlando Camargo Rodríguez

FIG. 5. Eigenray predictions for the ASP-H1 configuration: TRACEO, flat waveguide (top); TRACEO3D, cross-slope propagation on the wedge wave-guide (bottom). Source and receiver depth corresponds to 6.7 m and 11.0 m, respectively.

predictions, unsurprisingly, were found to be valid only close to the source. The proposed method allows an efficient and accurate calculation of 3D eigenrays by determining values of the corresponding take-off angles, which lead to the shooting of rays passing as close as desired to the position of a given receiver after multiple boundary reflections. Minor discrepancies found in the comparisons against experimental results are believed to be related to signal processing issues, and to ray theory being applied on the edge of its validity. Yet such discrepancies are completely independent of the proposed method of eigenray search, which was found to be extremely efficient and robust.

Future work will be oriented to the calculation of eigenrays in typical ocean environments, with complex bathymetries like sea canyons, or complex sound speed fields like the one produced by an upwelling regime. There are also theoretical methods that can be incorporated into the TRACEO3D model in order to improve its accuracy at those frequencies, which are considered too low for classical ray theory to be applied. Finally, to reduce significantly the time of computations, a parallel version of TRACEO3D based on the architecture of graphic processing units is currently underway.

ACKNOWLEDGMENTS

Buckingham, M. J. (**1987**). "Theory of three-dimensional acoustic propagation in a wedgelike ocean with a penetrable bottom," J. Acoust. Soc. Am. **82**(1), 198–210.

Calazan, R. M., Rodríguez, O. C., and Nedjah, N. (**2017**). "Parallel ray tracing for underwater acoustic predictions," in *Proceedings of the 17th ICCSA2017*, July 3–6, Trieste, Italy, Vol. 10404, pp. 43–55.

Červený, V., and Pšenčík, I. (**1979**). "Ray amplitudes of seismic body waves in laterally inhomogeneous media," Geophys. J. Int. **57**(1), 91–106.

Collins, M. D., and Kuperman, W. (**1991**). "Focalization: Environmental focusing and source localization," J. Acoust. Soc. Am. **90**(3), 1410–1422.

Gluk, Y., and Heyman, E. (**2011**). "Pulsed beams expansion algorithms for time-dependent point-source radiation. a basic algorithm and a standard-pulsed-beams algorithm," IEEE Trans. Antennas Prop. **59**(4), 1356–1371.

Harrison, C. H. (**1979**). "Acoustic shadow zones in the horizontal plane," J. Acoust. Soc. Am. **65**(1), 56–61.

Heilpern, T., Heyman, E., and Timchenko, V. (**2007**). "A beam summation algorithm for wave radiation and guidance in stratified media," J. Acoust. Soc. Am. **121**(4), 1856–1864.

Jensen, F. B., Kuperman, W. A., Porter, M. B., and Schmidt, H. (**2011**). *Computational Ocean Acoustics*, 2nd ed. (Springer Science & Business Media, New York), Chap. 3, pp. 155–226.

Korakas, A., Sturm, F., Sessarego, J.-P., and Ferrand, D. (**2009**). "Scaled model experiment of long-range across-slope pulse propagation in a penetrable wedge," J. Acoust. Soc. Am. **126**(1), EL22–EL27.

Lagarias, J. C., Reeds, J. A., Wright, M. H., and Wright, P. E. (**1998**). "Convergence properties of the Nelder–Mead Simplex method in low dimensions," SIAM J. Optim. **9**(1), 112–147.

Maltsev, N. (**2001**). "Enhanced ray theory," J. Comput. Acoust. **9**(1), 169–182.

Nelder, J. A., and Mead, R. (**1965**). "A simplex method for function minimization," Comput. J. **7**(4), 308–313.

Popov, M. M. (**2002**). *Ray Theory and Gaussian Beam Method for Geophysicists* (EDUFBA, Salvador, Bahia), pp. 89–144.

Reilly, S. M., Potty, G. R., and Goodrich, M. (**2016**). "Computing acoustic transmission loss using 3D Gaussian ray bundles in geodetic coordinates," J. Comput. Acoust. **24**(1), 1650007.

Rodriguez, O. C., Collis, J. M., Simpson, H. J., Ey, E., Schneiderwind, J., and Felisberto, P. (**2012**). "Seismo-acoustic ray model benchmarking against experimental tank data," J. Acoust. Soc. Am. **132**(2), 709–717.

Rodriguez, O. C., Sturm, F., Petrov, P., and Porter, M. (**2017**). "Three-dimensional model benchmarking for cross-slope wedge propagation," in *Proceedings of Meetings on Acoustics*, June 25–29, Boston, MA, Vol. 30, p. 070004.

Sturm, F., and Korakas, A. (**2013**). "Comparisons of laboratory scale measurements of three-dimensional acoustic propagation with solutions by a parabolic equation model," J. Acoust. Soc. Am. **133**(1), 108–118.

Tolstoy, A. (**1996**). "3-D propagation issues and models," J. Comput. Acoust. **4**(3), 243–271.

Weinberg, H., and Burridge, R. (**1974**). "Horizontal ray theory for ocean acoustics," J. Acoust. Soc. Am. **55**(1), 63–79.

Xing, C.-X., Song, Y., Zhang, W., Meng, Q.-X., and Piao, S.-C. (**2013**). "Parallel computing method of seeking 3D eigen-rays with an irregular seabed," in *Proceedings of Acoustics in Underwater Geosciences Symposium (RIO Acoustics)*, July 24–26, Rio de Janeiro, Brazil, pp. 1–5.